GS0613

インプットシェーピングによるクアッドローター吊り下げ荷物の振子運動抑制制御

Oscillation Suppression Control of a Quadrotor-borne Payload Using Input Shaping

○市川　サラ[*1]，小島　広久[*1]
Sarah ICHIKAWA[*1], Hirohisa KOJIMA[*1]
[*1] 首都大学東京　Tokyo Metropolitan University

Recently, expansion of drone applications has been expected, and payload delivery using drones is one such application. In this study, we consider a case in which a quadrotor carries a suspended payload and investigate a control scheme to eliminate oscillation of the payload caused by quadrotor maneuvers. We assume a model that has an offset between the suspension point and the center of mass of the quadrotor and derive the equations of motion. The input shaping technique is applied to the velocity control of the quadrotor to suppress the payload oscillation. Finally, the effectiveness of the input-shaping-based velocity control for payload oscillation suppression is verified through numerical simulations.

Key Words : Quadrotor, Input Shaping, Suspended Payload, UAV, Aerial Transportation

1. Introduction

Quadorotors have several applications, and transporting a payload suspended from a cable has been investigated. However, carrying a suspended payload by a quadrotor is problematic in that maneuvering of the quadrotor induces oscillation of the payload. Payload oscillation can damage the payload or affect quadrotor maneuvers. Hence, it is necessary to establish a control method that is stable and can eliminate oscillations. In this paper, in order to address the above problem, an input shaping approach that pre-generates commands in order to cancel residual oscillation is considered.

Homolka et al.(1) applied input command shapers to a two-dimensional quadrotor model. In 2017, Sadr et al.(2) developed a model-based algorithm (MBA) controller combined with an anti-swing controller based on input shaping. They examined the use of the zero vibration (ZV) shaper and the zero vibration and derivative (ZVD) shaper. In this paper, we extend their research by analyzing oscillation suppression for a wider variety of input shapers.

2. Dynamic Modeling

2・1 Coordinate definition and transformation

A model of the quadrotor with a suspended payload and the definitions of angles are shown in Fig. 1. The position of the quadrotor in the inertial frame is $\boldsymbol{r} = [\boldsymbol{x}\ \boldsymbol{y}\ \boldsymbol{z}]^{\boldsymbol{T}}$, and the attitude of the quadrotor is represented in the form of Euler angles $\boldsymbol{\xi} = [\boldsymbol{\phi}\ \boldsymbol{\theta}\ \boldsymbol{\psi}]^{\boldsymbol{T}}$, where the angles denote pitch, roll, and yaw, respectively.

The Z-X-Y rotational matrix from the body frame of the quadrotor to the inertial frame, $\boldsymbol{R}$, is

$$\boldsymbol{R} = \begin{bmatrix} \boldsymbol{c_\theta c_\psi - s_\phi s_\theta s_\psi} & \boldsymbol{-c_\phi s_\psi} & \boldsymbol{c_\psi s_\theta + c_\theta s_\phi s_\psi} \\ \boldsymbol{c_\theta s_\psi + c_\psi s_\phi s_\theta} & \boldsymbol{c_\phi c_\psi} & \boldsymbol{s_\psi s_\theta - c_\psi c_\theta s_\phi} \\ \boldsymbol{-c_\phi s_\theta} & \boldsymbol{s_\phi} & \boldsymbol{c_\phi c_\theta} \end{bmatrix} \tag{1}$$

where $c_x = \cos(x)$ and $s_x = \sin(x)$.

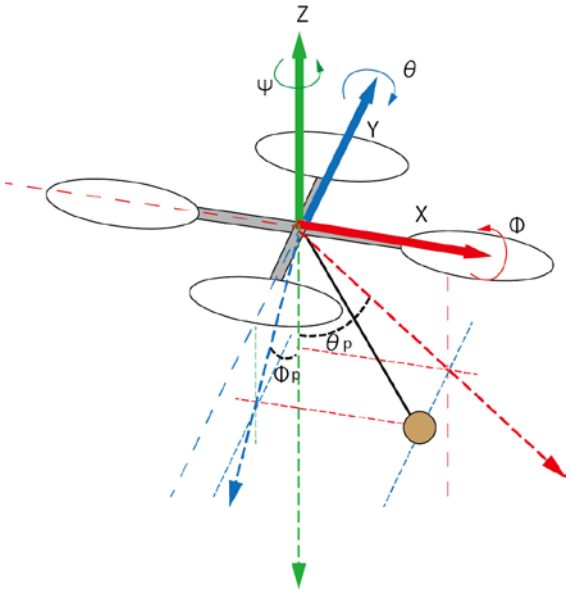

Fig. 1. Quadrotor with a suspended payload.

2・2 Control input

The control input consists of the total thrust of the quadrotor $\boldsymbol{T}$ and the torque $\boldsymbol{\tau}$, which are expressed as follows:[3]

$$\boldsymbol{T} = \boldsymbol{k_1\omega_1^2} + \boldsymbol{k_2\omega_2^2} + \boldsymbol{k_3\omega_3^2} + \boldsymbol{k_4\omega_4^2} \tag{2}$$

$$\boldsymbol{\tau} = \begin{bmatrix} \boldsymbol{\tau_\phi} \\ \boldsymbol{\tau_\theta} \\ \boldsymbol{\tau_\psi} \end{bmatrix} = \begin{bmatrix} \boldsymbol{lk_1\omega_3^2 - lk_3\omega_1^2} \\ \boldsymbol{lk_2\omega_4^2 - lk_4\omega_2^2} \\ \boldsymbol{b_1\omega_1^2 - b_2\omega_2^2 + b_3\omega_3^2 - b_4\omega_4^2} \end{bmatrix} \tag{3}$$

where $\boldsymbol{k_i}$, $\boldsymbol{\omega_i}$, and $\boldsymbol{b_i}$ are the thrust coefficient, the angular velocity, and the torque coefficient, respectively, of each motor, and $\boldsymbol{l}$ is the distance from the center of mass of the quadrotor to the center of the motor.

2・3 Quadrotor with a suspended payload dynamics

Since we assume that the quadrotor operates indoors, we neglect the effects of disturbances such as wind. Moreover, we adopt the model used in Nicholas' thesis.[4] The translational and rotational dynamics equations of the quadrotor are expressed as follows:

$$\ddot{\boldsymbol{r}} = \frac{\boldsymbol{1}}{\boldsymbol{m_q}}(\boldsymbol{F_g} + \boldsymbol{F_d} + \boldsymbol{RT_r} + \boldsymbol{RF_p}) \tag{4}$$

$$\ddot{\boldsymbol{\xi}} = \boldsymbol{I^{-1}}\ (\boldsymbol{\tau_d} + \boldsymbol{\tau} + \boldsymbol{\tau_p} - \dot{\boldsymbol{\xi}} \times (\boldsymbol{I}\,\dot{\boldsymbol{\xi}})) \tag{5}$$

where $\boldsymbol{m_q}$ is the mass of the quadrotor, $\boldsymbol{F_g}$ is the gravitational force, $\boldsymbol{F_d}$ is the drag force vector, $\boldsymbol{T_r}$ is the thrust vector, $\boldsymbol{F_p}$ is the payload tension, $\boldsymbol{I}$ is the moment of inertia of the quadrotor, $\boldsymbol{\tau_d}$ is the torque caused by drag, and $\boldsymbol{\tau_p}$ is the torque generated by the payload tension. Here, $\boldsymbol{F_g}, \boldsymbol{F_d}, \boldsymbol{T_r}, \boldsymbol{\tau_d}$, and $\boldsymbol{\tau_p}$ are given by

$$\boldsymbol{F_g} = \begin{bmatrix} \boldsymbol{0} & \boldsymbol{0} & \boldsymbol{-m_q g} \end{bmatrix}^{\boldsymbol{T}},\ \boldsymbol{F_d} = -\frac{\boldsymbol{1}}{\boldsymbol{2}}\boldsymbol{C_d\,A\,\rho_{air}}\ |\dot{\boldsymbol{r}}|\,\dot{\boldsymbol{r}},\ \boldsymbol{T_r} = [\boldsymbol{0}\ \boldsymbol{0}\ \boldsymbol{T}]^{\boldsymbol{T}},\ \boldsymbol{\tau_d} = \left(\boldsymbol{Rr_{cop}}\right) \times \boldsymbol{F_d}\ ,\ \boldsymbol{\tau_p} = \left(\boldsymbol{Rr_{susp}}\right) \times \boldsymbol{F_p} \tag{6}$$

where $\boldsymbol{g}$ is the gravitational acceleration in the inertial frame, $\boldsymbol{C_d}$ is the drag coefficient, $\boldsymbol{A}$ is the exposed area that generates drag, $\boldsymbol{\rho_{air}}$ is the air density, $\boldsymbol{r_{cop}}$ is the relative vector from the center of pressure to the center of gravity of the quadrotor in the body frame, and $\boldsymbol{r_{susp}}$ is the suspension offset in the body frame. Finally, $\boldsymbol{F_p}$ can be expressed as follows based on the small angle approximation:

$$\boldsymbol{F_p} = -\boldsymbol{m_p g_\xi} \tag{7}$$

where $\boldsymbol{m_p}$ is the payload mass, and $\boldsymbol{g_\xi}$ is relative gravitational acceleration.

3. Controller

3・1 Input shaping

Input shaping is a technique that can reduce oscillations when the period of oscillations is known. The period T_d can be expressed as $T_d = 2\pi\sqrt{L_p/g}$, where L_p is the length of the cable from which the payload is suspended. The general concept of input shaping, ZV shaper, which consists of two impulsive inputs, is explained here. The first impulse causes the system to vibrate, and the second impulse, the amplitude of which is the same as that of the first impulse, cancels the vibration.[5] The second impulse must be given to the system at the appropriate time, which is half the period of the oscillation. Impulse vectors are referred to as shapers, and input shaper command is generated by convolving the input shaper with the input command.

In this study, the ZV shaper command, negative zero-vibration (NZV) command, extra intensive (EI) command, and 2-hump EI shaped command were investigated for the oscillation control of the payload. Let the ratio of the amplitude of the impulse to the actual command be A_i and let the timing of the impulse be t_i, where i is the index.

The NZV shaper has two positive impulses and a negative impulse between the two positive impulses. The NZV shaper finishes all of the impulses within one third of one period by applying a negative impulse. Although the EI shaper requires the same duration as one period of oscillation, it is a robust shaper that allows a decent amount of modeling parameter uncertainty. Moreover, the EI shaper has a total of three impulses and contains a tolerable value limit V_{tol} on the percentage residual oscillations. The 2-hump EI shaper is an extended version of the EI shaper and has two humps in the sensitivity curve.

The amplitude and timing for the above shapers are written in matrix form in Eqs. (8) and (9).

$$ZV\ shaper \begin{bmatrix} A_i \\ t_i \end{bmatrix} = \begin{bmatrix} 0.5 & 0.5 \\ 0 & \frac{T_d}{2} \end{bmatrix},\ NZV\ shaper \begin{bmatrix} A_i \\ t_i \end{bmatrix} = \begin{bmatrix} 1 & -1 & 1 \\ 0 & \frac{T_d}{6} & \frac{T_d}{3} \end{bmatrix} \tag{8}$$

$$EI\ shaper \begin{bmatrix} A_i \\ t_i \end{bmatrix} = \begin{bmatrix} \frac{1+V_{tol}}{4} & \frac{1-V_{tol}}{2} & \frac{1+V_{tol}}{4} \\ 0 & \frac{T_d}{2} & T_d \end{bmatrix}, hump\ EI\ shaper \begin{bmatrix} A_i \\ t_i \end{bmatrix} = \begin{bmatrix} A_1 & \frac{1}{2}-A_1 & \frac{1}{2}-A_1 & A_1 \\ 0 & \frac{T_d}{2} & T_d & \frac{3}{2}T_d \end{bmatrix} \tag{9}$$

$$A_1 = (3X^2 + 2X + 3V_{tol}^2)/16X\ \ where,\ \ X = \sqrt[3]{V_{tol}^2(\sqrt{1-V_{tol}^2}+1)} \tag{10}$$

3・2 Quadrotor controller

This section describes the control methods used in the simulations. The quadrotor used in the simulations is assumed to have a PD attitude controller, a P velocity controller in the x- and y-directions, and a PID altitude controller. The controller scheme is shown in Fig. 2. Subscripts $wp, sp,$ and des denote waypoint, setpoint, and desirable, respectively. The gains for each controller are shown in Tables 1, 2, and 3. The physical parameters used for the simulations are listed in Table 4.

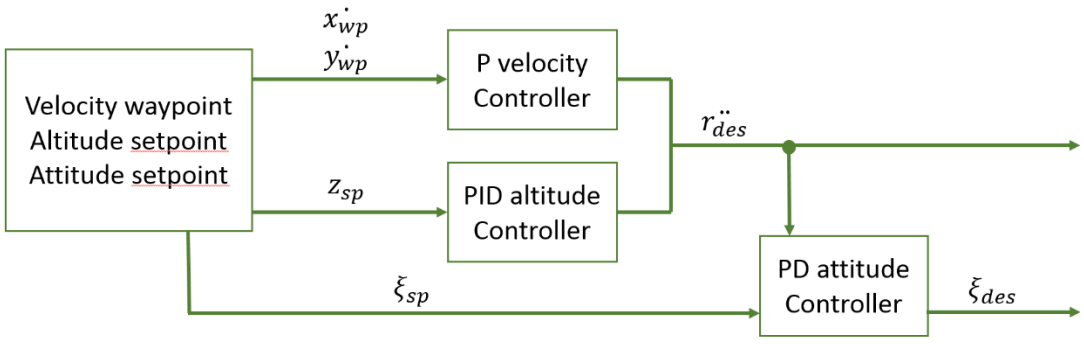

Fig. 2. Quadrotor controller scheme.

Table 1. PD attitude controller gains.

Gain	Value
K_{Px}	0.90
K_{Py}	0.90
K_{Pz}	0.90
K_{Dx}	0.28
K_{Dy}	0.28
K_{Dz}	0.28

Table 2. P velocity controller gains.

Gain	Value
K_{Px}	1.2
K_{Py}	1.2
K_{Pz}	0

Table 3. PID altitude controller gains.

Gain	Value
K_{Px}	12
K_{Py}	12
K_{Pz}	30
K_{Ix}	1
K_{Iy}	1
K_{Iz}	1
K_{Dx}	6
K_{Dy}	6
K_{Dz}	6

Table 4. Physical parameters used in the simulations.

Parameter	Value
$m_q(kg)$	1
$I_{xx}(kg/m^2)$	$6{,}815{,}763.88t10^{-9}$
$I_{yy}(kg/m^2)$	$6{,}801{,}641.50t10^{-9}$
$I_{zz}(kg/m^2)$	$4{,}548{,}279.56t10^{-9}$
$l(m)$	0.15546
C_d	1
$A(m^2)$	0.025
$\rho_{air}(kg/m^3)$	1.22
$r_{cop}(m)$	$[0\ 0\ 0.05]^T$
$r_{susp}(m)$	$[0\ 0\ 0.02]^T$
$m_p(kg)$	0.073

4. Simulation Results

In the simulations, the maximum translational velocity is limited to $0.5\,(m/s)$, and the maximum translational acceleration of the quadrotor is limited to $5\,(m/s^2)$ because a real quadrotor cannot exactly respond to bang-bang control. In this simulation, the quadrotor followed a straight trajectory that is 2 m long in the y-direction. The velocity profiles of the quadrotor with a cable of length $L_p = 0.5$ (m) for the non-shaped command for the various shapers are shown in Fig. 3. The effect of L_p on the residual vibration amplitude of payload angles as seen from the body frame is shown in Fig. 4. Figure 5 shows the time histories of the y-direction velocity of the quadrotor for several cable lengths for the 2-hump EI shaper.

As shown in Fig. 4, all of the shapers suppress residual vibration better than unshaped control. The residual vibration amplitude for the EI shaper is larger than those of the other shapers when L_p is less than 0.4. On the other hand, when L_p is greater than 0.4, the other three shapers exhibit a larger residual vibration amplitude than the EI shaper. The EI shaper is shown to be less sensitive to higher frequencies, and the ZV, NZV, and 2-hump EI shapers are less sensitive to lower frequencies. In the case of a longer cable, the residual vibration amplitude for the 2-hump EI shaper becomes larger than those of the other three shapers because the velocity profile of the 2-hump EI shaper changes more quickly as L_p increases. As shown in Fig. 5, the velocity profile is not tracked accurately when $L_p > 0.9$ because the velocity profile changes too quickly. In the maximum velocity is not reached, the appropriate amplitude impulse cannot be applied. As a result, oscillation cancellation will not be achieved.

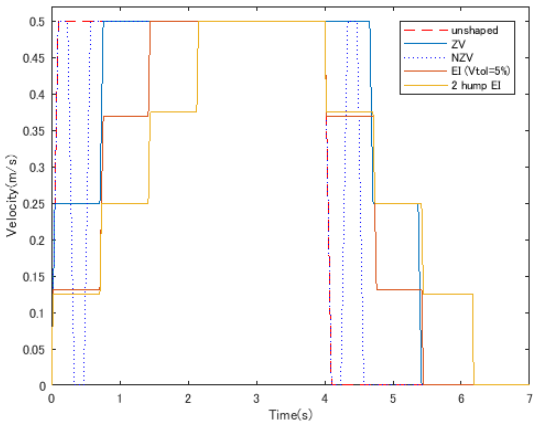

Fig. 3. Velocity profiles for each shaper.

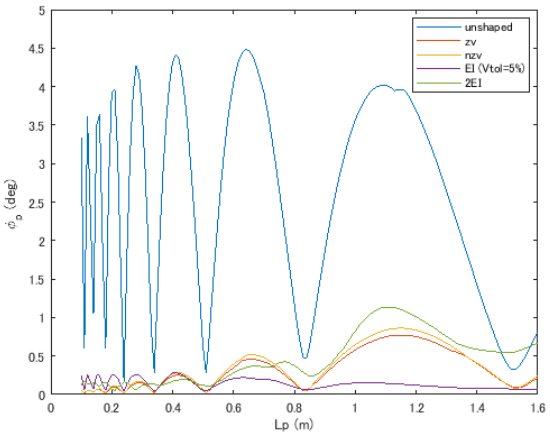

Fig. 4. Effect of L_p on residual vibration amplitude.

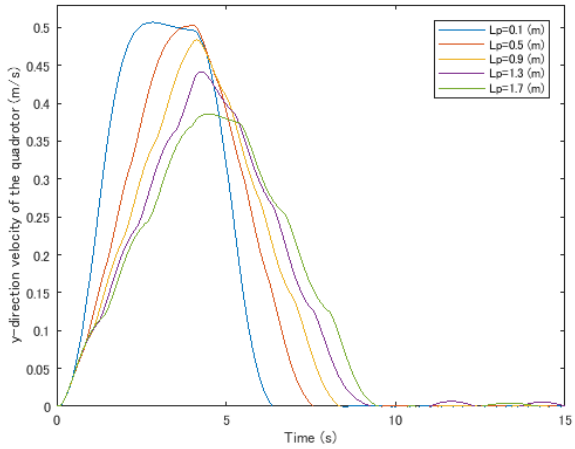

Fig. 5. Time histories of y-direction velocity of the quadrotor.

5. Conclusions and Future Work

The primary objective of the present study was to implement input shaping in quadrotor control and to verify that the modified control can eliminate oscillations of a cable-suspended payload attached to a quadrotor. A model of the dynamics of the quadrotor with a suspended payload was developed, and several types of input shapers were applied to velocity control of the quadrotor. The numerical simulations indicate that implementing input shaping in velocity control reduced payload oscillation. Since this technique has not been tested on an actual quadrotor, experiments should be carried out as future work.

References

(1) Homolka. P, Hrom. M. “Input Shaping Solutions for Drones with Suspended Load : First Results”, 21st International Conference on Process Control C)2017

(2) Sadr, S. Ali, S. Moosavian, A., and Zarafshan, P., “Dynamics Modeling and Control of a Quadrotor with Swing Load,” Journal of Robotics, Vol. 2014, Article ID 265897, 12 pages

(3) Derafa, L., Madani, T., and Benallegue, A., “Dynamic Modelling and Experimental Identification of Four Rotors Helicopter Parameters,” IEEE International Conference on Industrial Technology, pp. 1834-1839, 2006.

(4) Johnson, N., “Control of a Folding Quadrotor with a Slung Load Using Input Shaping” (Master thesis), 2017.

(5) O. J. M Smith, “Feedback Control Systems,” McGraw-Hill Book Company, Inc, 1958.

(6) W. E. Singhose, W. P. Seering, and N. C. Singer, “Time-Optimal Negative Input Shapers,” Journal of Dynamic Systems, Measurement, and Control, Vol. 119,p. 198, 1997.

(7) W. Singhose, W. Seering, and N. Singer, “Residual Vibration Reduction Using Vector Diagrams to Generate Shaped Inputs,” Journal of Mechanical Design, Vol. 116,no. 2, p. 654, 1994.

(8) W. Singhose, L. Porter, T. Tuttle, and N. Singer, “Vibration Reduction Using Multi-Hump Input Shapers,” Transactions of the ASME, Vol. 119, pp. 320–326, 1997.